Journal of Microscopy, Vol. 191, Pt 3, September 1998, pp. 286–296.
Received 30 May 1997; accepted 19 February 1998

Quantitative analysis of valence electron energy-loss spectra of aluminium nitride

A. D. DORNEICH,*† R. H. FRENCH,‡ H. MÜLLEJANS,*§ S. LOUGHIN† & M. RÜHLE*
**Max-Planck-Institut für Metallforschung, Seestraße 92, D-70174 Stuttgart, Germany*
‡DuPont Central Research, E356-384 Experimental Station, Wilmington, DE 19880, U.S.A.

Key words. Aluminium nitride, STEM, VEELS.

Summary

The optical properties and electronic structure of aluminium nitride are determined using valence electron energy-loss spectroscopy in a dedicated scanning transmission electron microscope. Quantitative analysis of the experimental valence electron energy-loss spectra to determine the electronic structure encompasses single scattering deconvolution of the valence electron energy-loss spectra to calculate the energy-loss function, Kramers–Kronig analysis of the energy-loss function to reveal the complex dielectric function, transformation of the dielectric function into the optical interband transition strength via optical property relations and finally critical-point analysis of the interband transition strength. The influence of both experimental and analytical parameters on the final result was studied systematically to define and improve the understanding of the methods. To check the reliability of this technique the interband transition strength determined was compared with results of vacuum ultraviolet spectroscopy. Good agreement was found if sample preparation was taken into account. The preparation of the specimen for the transmission electron microscopy has an effect on the electronic structure. Quantitative analysis of valence electron energy-loss spectroscopy, using the methods presented, is an important and capable method to determine the electronic structure of materials and it has the benefit of high spatial resolution.

1. Introduction

Basic properties of materials, such as optical, electrical and physical behaviour, are determined by the electronic structure of the material (French, 1990; Sutton, 1993; French *et al.*, 1994, 1995). Furthermore, knowledge of the electronic structure is important for the understanding of the bonding and forces at the atomic level (Ching, 1990). Recently, methods have been developed to determine the interband transition strength J_{CV}, which is the convolution of the valence and conduction band densities of states weighted by the dipole selection rule matrix elements. It can be obtained from optical spectroscopy or band structure calculations (Loughin *et al.*, 1996). Critical point analysis of these interband transition strength spectra can then be used for the comparison and interpretation of results from experimental and theoretical methods in terms of interband transitions between the valence and the conduction bands (Loughin *et al.*, 1996).

Valence electron energy-loss spectroscopy (VEELS) is another experimental technique for probing the electronic structure of materials (Raether, 1965; Daniels *et al.*, 1970; Fink, 1989). Walsh (1989) and others (Festenberg, 1969) have used electron energy-loss (EEL) spectra to obtain the dielectric function, ε, of a number of materials. Müllejans *et al.* (1993, 1994) have reported quantitative analysis of experimental EEL spectra in order to obtain the interband transition strength. VEELS can be performed in a scanning transmission electron microscope (STEM) to study the electronic structure with high spatial resolution owing to the subnanometre probe size. This technique has been used to analyse the electronic structure of the near-$\Sigma 11$ grain boundary in α-alumina (Müllejans & French, 1996) and of intergranular glassy films in Si_3N_4 (French *et al.*, 1998).

In this paper we will apply the concept of the interband transition strength J_{CV} to our VEELS results of aluminium nitride (AlN). Most parts of the analysis have been described previously, but the analysis has been validated and improved and will be completely described and presented in Section 4.

The analysis requires several steps such as the deconvolution of the multiple scattering EEL spectra and subsequent Kramers–Kronig analysis and one has to be alert

Correspondence to: R. H. French.
Present addresses: †Gebhard Balluf GmbH & Co., Gartenstraße 21–25, 73765 Neuhausen/Filder, Germany; §Institute for Advanced Materials, Joint Research Centre, European Commission, PO Box 2, NL-1755 ZG Petten, The Netherlands.

for artefacts which can be associated with analytical assumptions and parameters. A check on the reliability of the measurement and the analysis of VEELS is possible by the comparison of the final output results with those from other methods, such as vacuum ultraviolet (VUV) spectroscopy. For quantitative and accurate studies of the electronic structure of materials it is important to develop robust and diverse experimental and theoretical methods, apply them to the same materials and compare the results.

In this work therefore, VEELS was used to study the electronic structure of AlN. While a number of raw EEL-spectra of AlN (Lieske & Hezel, 1981; Olson *et al.*, 1985; Gautier *et al.*, 1987) are available, none of them have been analysed quantitatively to obtain J_{CV}. However, calculations of the band structure of AlN (Ching & Harmon, 1986) and experimental results from VUV-spectroscopy (Loughin *et al.*, 1993) are available. AlN is a material of great technological interest because it has high thermal conductivity and a thermal expansion coefficient similar to that of silicon which makes it suitable as a ceramic package for microcircuits (Werdecker & Aldinger, 1984).

2. Analysis of valence EELS: formalism

The physical background of how an experimental EEL-spectrum is related to the electronic structure of a material is the focus of this section. This forms the basis for the analytical methods described in Section 4. In the present paper the treatment is nonrelativistic, which is appropriate for energies up to ≈ 100 keV. The more general relativistic expressions can be found in Egerton (1996).

2.1. Inelastic electron scattering

In a STEM an electron beam is focused on a thin specimen. The transmitted beam electrons interact with the solid and some of them lose energy by inelastic scattering. EEL-spectra of the transmitted electrons are acquired with an electron energy-loss spectrometer and they contain information about the electronic structure and chemical composition of the specimen. There are distinct regions in an EEL-spectrum which can be related to different energy-loss mechanisms (Fig. 1). The dominant feature in an EEL-spectrum is the zero-loss peak (region 1) due to unscattered and elastically scattered electrons. The width of this peak at 0 eV reflects the energy width of the primary electrons and the resolution of the spectrometer. In this work the full width at half-maximum was about 0·7 eV. Therefore the zero-loss peak also includes phonon-scattered electrons, which have lost an amount of energy which is small relative to the resolution of the system. Region 2 (the low-loss or valence-loss region) contains electrons which have lost energy by excitation of a plasmon, a collective oscillation of the valence electrons, or by interband transitions of single electrons from the occupied valence band into the empty conduction band. At energies above 50 eV edges appear in the EEL-spectrum. They are caused by ionization of inner shell electrons and are therefore characteristic of the atomic elements in the specimen. In the case of AlN the aluminium $L_{2,3}$-edge appears at about 76·5 eV and the nitrogen K-edge at 400 eV. The K-edges of oxygen (532 eV) and carbon (284 eV) occur as a result of an oxide layer and of contamination on the specimen surface.

This work is focused on the low-loss, or valence-loss, region where the interband transitions are situated. In a

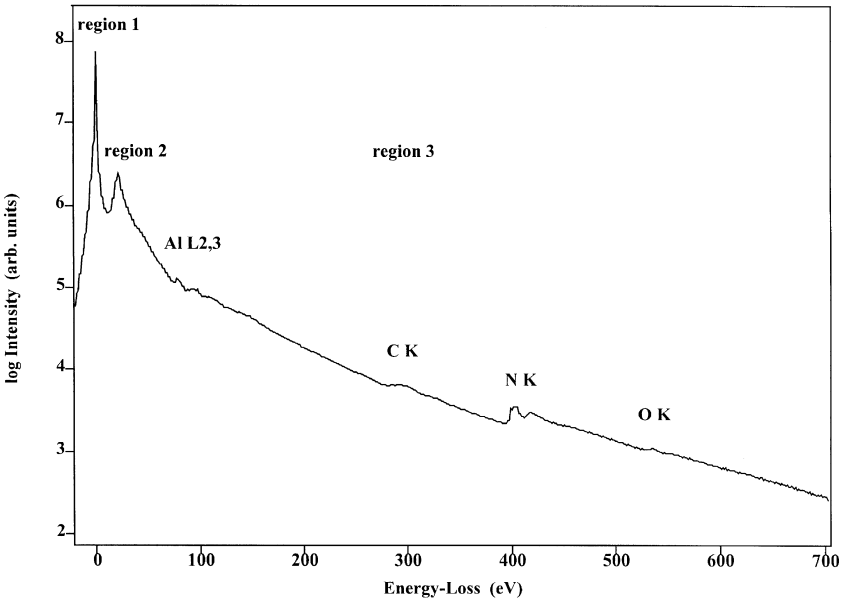

Fig. 1. Energy-loss spectrum of single-crystal AlN covering the zero-loss (1), low-loss (2) and core-loss (3) regions. The *y*-axis is on a logarithmic scale.

first step (Section 2.1.1) it will be shown that the EEL-spectrum containing only single scattering events is proportional to the energy-loss function which is defined as the imaginary part of $-1/\varepsilon(E)$ where E is the energy loss and ε is the complex dielectric function. The contributions of multiple scattering, which are always present in an experimental EEL-spectrum, are an undesirable complication but they can be removed by deconvolution (Section 2.1.2). To obtain the complex dielectric function $\varepsilon = \varepsilon_1 + i\varepsilon_2$ from $\mathrm{Im}(-1/\varepsilon)$, a Kramers–Kronig analysis is necessary (Section 2.2). Finally, because the optical properties are related to the electronic structure, the interband transition strength $J_{CV}(E)$ can be obtained from $\varepsilon(E)$ (Section 2.3).

2.1.1. Energy-loss function. The differential cross-section for scattering with an energy-loss E and a scattering angle θ can be calculated with the help of dielectric theory (Schattschneider, 1986). In an experiment, a range of scattering angles has to be taken into account because of the finite collector aperture of the spectrometer. Therefore, integration of the differential cross-section over the scattering angle θ, up to the collection semi-angle β of the spectrometer, results in an expression for the single scattering distribution $S(E)$:

$$S(E) = \frac{I_0 t}{\pi a_0 m_0 v^2} \mathrm{Im}\left(\frac{-1}{\epsilon(E)}\right) \ln\left(1 + \left(\frac{\beta}{\theta_E}\right)^2\right), \qquad (1)$$

where I_0 is the intensity of the unscattered or elastically scattered electrons, t the thickness of the specimen, a_0 the first Bohr radius, m_0 the electron mass and v the velocity of the incident electrons. The conservation of energy and momentum leads to an expression which relates the momentum transfer $\mathbf{q}$ to the energy-loss E and the scattering angle θ:

$$q^2 = k_0^2 (\theta^2 + \theta_E^2), \qquad (2)$$

where $\theta_E = (E/2E_0)$, k_0 is the momentum and E_0 the energy of the incident electron. θ_E is the characteristic scattering angle which has a value of 0·1 mrad for $E_0 = 100$ keV and $E = 20$ eV. Equation (1) assumes the dipole approximation, i.e. $\varepsilon(E, \mathbf{q}) = \varepsilon(E, \mathbf{0}) = \varepsilon(E)$ for small values of the momentum transfer $\mathbf{q}$ (Egerton, 1996). It is found here that this approximation is valid for values of β up to 13 mrad in the case of AlN. The imaginary part of $-1/\varepsilon(E)$ is known as the energy-loss function and provides a complete description of the response of the material to the fast electrons travelling through it.

The Lorentz oscillator is a simple model to describe the dielectric function $\varepsilon(\omega)$. For high frequencies, corresponding to high energy losses, the electrons behave as free particles and the interaction between the electrons is introduced by a damping constant Γ (Egerton, 1996). This approximation can be used to extrapolate the experimental data outside the measured energy interval before Kramers–Kronig analysis (Section 4.3). In the limit of high energies the optical properties obey certain power laws (Table 1).

2.1.2. Multiple scattering energy-loss spectrum. A transmitted electron can be scattered inelastically more than once, giving a total energy loss which is the sum of the individual losses. Because every scattering event can be viewed as independent of the preceding ones, the probability for an electron to suffer n collisions obeys the Poisson statistics. The contribution of the electrons which are scattered n times is therefore the n-fold convolution of the single scattering EEL-spectrum $S(E)$. The experimental EEL-spectrum $J(E)$ is an infinite sum of all these contributions. The prefactors can be derived from the Poisson distribution (Egerton, 1996):

$$\begin{aligned} J(E) &= R(E) * [I_0\delta(E) + S(E) + D(E) + T(E) + \ldots] \\ &= Z(E) * \left[\delta(E) + \frac{1}{I_0} S(E) + \frac{1}{2!I_0^2} S(E) * S(E) \right. \\ &\quad \left. + \frac{1}{3!I_0^3} S(E) * S(E) * S(E) + \ldots\right], \end{aligned} \qquad (3)$$

where $R(E)$ is the resolution function of the microscope and the spectrometer, * denotes convolution and $Z(E)$ is the experimentally observed zero-loss peak. $D(E)$ and $T(E)$ are the contributions of the double- and triple scattering events, respectively. I_0 is the number of the electrons under the zero-loss peak $Z(E)$ and $\delta(E)$ is the unit-area delta function. To extract $S(E)$ from the experimental spectrum $J(E)$, Eq. (3) is transformed to Fourier space:

$$j(v) = z(v) \cdot \left[1 + \frac{s(v)}{I_0} + \frac{s^2(v)}{2!I_0^2} + \ldots\right] = z(v) \cdot \exp\left(\frac{s(v)}{I_0}\right), \qquad (4)$$

where $j(v)$, $s(v)$ and $z(v)$ are the Fourier-transform of $J(E)$, $S(E)$ and $Z(E)$. v has units of eV^{-1}. The convolution becomes a product and $s(v)$ can be calculated as

$$s(v) = I_0 \ln [j(v)/z(v)]. \qquad (5)$$

Table 1. Power laws for the optical properties in the limit of high energies

Optical property	Power law
Complex dielectric constant $\varepsilon_1 + i\varepsilon_2$	$\varepsilon_1 = 1 - (\omega_p^2/\omega^2)$ $\varepsilon_2 = (\omega_p^2\Gamma)/(\omega^3)$
Energy-loss function	$\mathrm{Im}(-1/\varepsilon) = (\omega_p^2\Gamma)/(\omega^3)$

$\omega_p = \sqrt{(4\pi n e^2 m_0^{-1})}$ is the plasma frequency, n the electron density and Γ the damping constant.

2.2. Kramers–Kronig dispersion analysis

Because $\varepsilon(\omega)$ is a causal quantity the Kramers–Kronig (KK) relation (de Kronig, 1926; Kramers, 1927) can be formulated:

$$\mathrm{Re}\left[\frac{1}{\epsilon(E)}\right] = 1 - \frac{2}{\pi} P \int_0^\infty \mathrm{Im}\left[\frac{-1}{\epsilon(E')}\right] \frac{E' \mathrm{d}E'}{E'^2 - E^2}, \qquad (6)$$

where P denotes the Cauchy principal part of the integral.

The KK relation can be used to calculate the prefactor in Eq. (1) which cannot be determined from experiment because t is unknown. For $E = 0$ in Eq. (6):

$$1 - \frac{1}{n^2} = \frac{2}{\pi} P \int_0^\infty \mathrm{Im}\left[\frac{-1}{\epsilon(E')}\right] \frac{\mathrm{d}E'}{E'}. \qquad (7)$$

For small energies (< 1 eV) ε_2 is small and $\mathrm{Re}(1/\varepsilon) \cong 1/\varepsilon_1(0)$. $\varepsilon_1(0)$ can be taken as the square of the refractive index n for visible light since the experimental EEL-spectrum does not extend to 0 eV because of the limited energy resolution of the microscope and the spectrometer. After the prefactor in Eq. (1) has been determined with the help of the refractive index, the single scattering deconvolved spectrum can be scaled and the energy-loss function is then known on an absolute scale. In the next step $\mathrm{Re}(1/\varepsilon(E))$ is calculated from $\mathrm{Im}(-1/\varepsilon(E))$ with the help of the KK analysis (Eq. 6), and then $\varepsilon(E)$ is determined.

2.3. Optical property relations

2.3.1. Interband transition strength. In the last section it was shown that the dielectric function $\varepsilon(E)$ can be determined from an EEL-spectrum. Now, the relationship of the interband transition strength $J_{\mathrm{CV}}(E)$ to the dielectric constant $\varepsilon(E)$ is presented. We restrict ourselves to the case of an insulator with a filled valence band and an empty conduction band which are separated by the band gap. The energy loss of the fast electron is the energy transferred to the solid, which, sometimes, will be called energy in the following because of the analogy to photon absorption. The interaction of light with a solid can be described in terms of electronic band structure by Fermi's golden rule (Wooten, 1972). The transition rate between an initial state $|\mathrm{v}\rangle$ in the valence band and a final state $|\mathrm{c}\rangle$ in the conduction band W_{CV} is

$$W_{\mathrm{cv}} = \frac{e^2}{\epsilon_1 \pi m_0^2 \omega} \int \mathrm{d}\mathbf{k} \left|\mathbf{a_0} \cdot \mathbf{p}_{ij}\right|^2 \delta(E_{\mathrm{cv}} - \hbar\omega), \qquad (8)$$

where $E_{\mathrm{CV}}(\mathbf{k}) = E_{\mathrm{c}}(\mathbf{k}) - E_{\mathrm{v}}(\mathbf{k})$ is the energy difference between the conduction band and the valence band, $\mathbf{a_0}$ is the polarization vector of the light and $\mathbf{p}_{ij}$ is the matrix element of the momentum. $\hbar\omega$ is the photon energy, m_0 the electron mass and e the electron charge. An expression for the absorption coefficient is obtained by expressing the power absorption as the quantum mechanical transition rate W_{CV} times the energy $\hbar\omega$ absorbed per transition. An equation for ε_2 that follows from this relationship is (Wooten, 1972)

$$\varepsilon_2 = \varepsilon_1 W_{\mathrm{CV}} / \omega. \qquad (9)$$

The integral in Eq. (8) can be transformed into a surface integral; the integration has to be performed over the surface in the $\mathbf{k}$-space where $E_{\mathrm{CV}}(\mathbf{k}) = \hbar\omega$. If it is assumed that the factor $|\mathbf{a_0} \cdot \mathbf{p}_{ij}|$ in Eq. (8) varies only slowly with energy it can be taken outside the integral. The remaining integral is well known as the joint density of states J'_{CV}:

$$J'_{\mathrm{cv}} = \frac{1}{8\pi^3} \int \frac{\mathrm{d}S}{\left|\nabla_k E_{\mathrm{cv}}(k)\right|_{\hbar\omega}}. \qquad (10)$$

The product of the joint density J'_{CV} of states and the square of the matrix element $|\mathbf{a_0} \cdot \mathbf{p}_{ij}|$ is the interband transition strength $J_{\mathrm{CV}}(E)$ and takes the dipole selection rules for the transitions into account. $J_{\mathrm{CV}}(E)$ is proportional to the probability that a transition of an electron between the filled valence band and empty conduction band with the transition energy E takes place. Using Eqs. (8), (9) and (10) $J_{\mathrm{CV}}(E)$ can be related to $\varepsilon(\omega)$:

$$J_{\mathrm{cv}}(E) = \left|\mathbf{a_0 p}_{ij}\right|^2 J'_{\mathrm{cv}}(E) = \frac{m_0^2}{e^2\hbar^2} \frac{E^2}{8\pi^2} (\epsilon_2(E) + i\epsilon_1(E)). \qquad (11)$$

The imaginary part of $J_{\mathrm{CV}}(E)$ arises from dispersive processes (Loughin *et al.*, 1996). The joint density of states has units of $\mathrm{cm}^{-3}\,\mathrm{eV}^{-1}$ because this quantity counts the number of states per crystal volume and energy interval. The matrix element has units of momentum and therefore, according to Eq. (11), the interband transition strength $J_{\mathrm{CV}}(E)$ has units of density. For computational convenience we take the prefactor $m_0^2 e^{-2} \hbar^{-2}$ in Eq. (11) whose value in cgs units is $8{\cdot}289 \times 10^{-6}\,\mathrm{g\,cm^{-3}\,eV^{-2}}$ as unity. Therefore the $J_{\mathrm{CV}}(E)$ spectra plotted in this paper have units of eV^2.

2.3.2. Critical point analysis. Major contributions to the interband transition strength $J_{\mathrm{CV}}(E)$ occur when $|\nabla_{\mathrm{k}} E_{\mathrm{CV}}(k)| = 0$ (Eq. 10). Points in $\mathbf{k}$-space where this condition is fulfilled are called critical points or van Hove singularities. In the vicinity of a critical point the interband energy can be approximated with a quadratic form

$$E_{\mathrm{CV}}(k) = E_0 + \beta_1 k_1^2 + \beta_2 k_2^2 + \beta_3 k_3^2. \qquad (12)$$

The number of non-vanishing coefficients determines the dimensionality n_{j} of the jth critical point. The types of critical point (maximum, saddle point, minimum) correspond to the possible choices of signs for the coefficients β_1, β_2 and β_3. In the 3D case the critical points are labelled M_0, M_1, M_2 and M_3. For the 2D and 1D band

system they are denoted D_0, D_1 and D_2 and P_0 and P_1, respectively, while a 0D band system is denoted S_0. A model of a real electronic structure may be constructed by summing together the contributions from individual critical points. Each feature in an experimental $J_{CV}(E)$ spectrum has to be described by a balanced set of critical points (Loughin, 1992; Loughin *et al.*, 1996). A balanced set consists of a number of critical points such that outside the energy range over which transitions can occur the model predicts a vanishing optical response. Therefore the line shape of the critical points used for a set have to cancel outside the interesting range. A computer program (Loughin *et al.*, 1996) was used for optimizing the parameters of the critical point model.

2.3.3. Sum rule. From theory of quantum mechanics a sum rule (Smith, 1985) can be formulated for the interband transition strength $J_{CV}(E)$. $n_{eff}(E)$ is the number of electrons contributing to a transition up to an energy E:

$$n_{eff}(E) = \frac{4v_f}{m_0}\int_0^E \frac{J_{cv}(E')}{E'}\,dE', \qquad (13)$$

where v_f is the volume of one formula unit whose value is $20{\cdot}86\ \text{Å}^3$ for AlN. From Eq. (13) one can see that the units of density for J_{CV} correspond to the mass of electrons per unit volume. In the limit of $E \rightarrow \infty$ n_{eff} is the number of valence electrons per formula unit which is 8 for AlN. Equation (13) can be applied to single sets of critical points to determine how many electrons are involved in the respective transition.

3. Experimental methods

3.1. Sample preparation

3.1.1. AlN materials. For the VEELS-experiment a single crystal AlN specimen was used. The specimen was supplied by General Electric Company and cut from a single boule of AlN which was grown by Slack (1973). Slack found a thermal conductivity of $275\ \text{W m}^{-1}\text{K}^{-1}$ and an oxygen concentration of 340 p.p.m. by neutron activation.

3.1.2. TEM foil preparation. The TEM foil was prepared by standard methods. A disc (3 mm in diameter) was thinned mechanically with diamond paste suspended in water. After this step the specimen was dimpled to a residual thickness in the centre of the disc of about 20 μm. The specimen was then thinned by an argon ion beam of an energy of 6 keV under an angle of 12° in a Gatan ion mill until perforation (about 8 h). The specimens were examined uncoated. Nevertheless specimens did not charge during investigation in the STEM.

3.2. Data acquisition

The VEELS experiments were performed with a parallel electron energy-loss spectrometer (PEELS) (Gatan 666) fitted to a dedicated STEM (Vacuum Generator HB501) operating at 100 keV. The PEELS consists of a magnetic prism, quadrupole lenses, a scintillator and a photodiode array for parallel recording of 1024 channels. The microscope is equipped with a high-resolution pole piece and a cold field emission electron source. The beam was focused to less than 1 nm diameter. Spectra were acquired while the beam was scanning an area of 10 nm × 12 nm. The system had an energy resolution of 0·7 eV, indicated by the full width at half-maximum of the zero-loss peak (Fig. 1). The energy dispersion of the spectrometer was 0·1 eV per channel. To avoid a cut-off effect at the left end of the spectrum 0 eV was positioned at channel 200. The detector saturates at 16 384 counts. Because the EEL-spectrum has a high dynamic range (5 decades in Fig. 1) some channels at the minimum between the zero-loss peak and the plasmon peak contain a low number of counts and have therefore a low signal-to-noise ratio (SNR) (Egerton *et al.*, 1993). The possibility of increasing SNR by the acquisition and summation of a large number of spectra is limited because of the danger of radiation damage and instabilities of the microscope and the spectrometer in case of long exposure times. To improve the SNR in this region where the interband transitions occur two spectra were taken at the same position on the specimen. The zero-loss optimized spectrum was taken with a short acquisition time (0·05 s) such that the zero-loss peak was not saturated and a complete spectrum was obtained. A second spectrum was acquired with a longer exposure time (2·0 s) such that the plasmon peak was just below saturation. This one is plasmon-loss optimized and the channels corresponding to the low-loss region contain more counts and therefore less noise. Since the plasmon-loss optimized spectrum is saturated in the zero-loss region it has to be spliced together with the zero-loss optimized spectrum to get a complete EEL-spectrum with a sufficient SNR. The convergence and collection semi-angle were varied systematically in this work. It was found that 25 mrad and 13 mrad, respectively, were good choices in order to gather sufficient electrons and reduce the SNR while minimizing the radiation damage.

4. Analytical methods and results

4.1. Correction of the detector characteristic

First the measured EEL-spectrum was corrected for the readout pattern and the dark current of the photodiode. For this, a dark current spectrum was taken with the same acquisition time but without the electron beam and subtracted from the EEL-spectrum. To correct the

channel-to-channel gain variation, the real spectrum is divided by the gain spectrum which is recorded when the diode array is evenly illuminated by an undispersed beam. These procedures, as well as the control of the PEELS, were performed on a Macintosh computer using EL/P.[1] The following steps of the analysis were performed on an IBM compatible 486 PC using GRAMS.[2]

4.2. Single scattering deconvolution

The zero-loss optimized and the plasmon-loss optimized spectra are spliced together such that the second spectrum is replaced by the first where it is saturated. In order to find the best fit the zero-loss spectrum is not only scaled by a factor but also the energy scale is shifted with respect to the plasmon-loss optimized spectrum to compensate for instabilities of the spectrometer.

Starting from the spliced spectrum $J(E)$ the next step is to obtain the single scattering distribution $S(E)$. Several implementation methods for deconvolution of the recorded spectrum containing contributions from multiple scattering have been described by Egerton (1996). The commercial software package El/P from Gatan has incorporated one of the basic routines. The assumptions made are that the zero loss peak is symmetric, so that the negative side of the energy axis can be mirrored to the positive side and can be used as a zero-loss peak shape. Furthermore, the experimental data are considered only above the first minimum between zero loss and plasmon loss, the data below being replaced by a linear extrapolation to zero intensity at the origin of the energy scale. These simplifications do not change the results of single scattering deconvolution for energies above the plasmon peak. The results in the band gap region and just above, however, critically depend on these assumptions. Since this energy range is important for the determination of the optical properties, we have developed an improved treatment of this problem which is outlined in the following.

Because of the finite energy resolution of the spectrometer it is impossible to recover an unbroadened single scattering distribution. Therefore $s(v)$ in Eq. (5) is to be reconvolved by $Z(E)$ before inverse Fourier-transformation (Egerton, 1996). To obtain $Z(E)$ the experimental data $J(E)$ are used up to a boundary energy and are replaced by an analytic function for higher energies. The band gap energy of the material can be taken as an upper limit for the boundary energy since there is no contribution of inelastic scattering expected below the band gap energy. Because $J_{CV}(E)$ is zero in the band gap, ε_2 as well as $\mathrm{Im}(-1/\varepsilon)$ vanish (Eq. 11). In the case of AlN, 4 eV was used as the boundary energy, which is below the band gap of 6·3 eV. Because the zero-loss peak is asymmetric, $Z(E)$ is approximated by an asymmetric Pearson VII peak shape[3] (Johnson & Kotz, 1970). Fitting the experimental data to an analytic function is a way of finding the origin of the energy scale (i.e. 0 eV). One advantage of the GRAMS software is that it is not restricted to coarse energy channels but fitting and shifting are possible in parts of the energy increment. After $Z(E)$ has been determined $z(v)$ and $j(v)$ are generated by a fast Fourier-transformation (FFT). The logarithm is taken following Eq. (5) and the phases are adjusted as described elsewhere (Egerton, 1996). The result is then multiplied by $z(v)$ to reconvolve this function and an inverse FFT is applied to obtain $S(E)$ (Fig. 2). The single scattering deconvolution assumes an infinite collection angle. Comparison between results from data acquired under a variety of combinations of incident and collection semi-angles suggested that there was only a minor influence on the computed results. The single scattering deconvoluted data did not give any indication of residual multiple scattering components.

The relative thickness $t/\lambda = \ln(I_t/I_0)$ can be calculated after the single scattering deconvolution because I_0, the integral under the $Z(E)$, and I_t, the integral under $J(E)$ are available. Combining Eqs (1) and (7), the absolute thickness t and the mean free path λ can be determined. The mean free path for AlN was found to be $\lambda = 102$ nm and the thickness at the position on the specimen where the EEL-spectrum (Fig. 1) was acquired was $t = 99{\cdot}5$ nm.

4.3. Kramers–Kronig analysis

Before $\mathrm{Re}(1/\varepsilon)$ is obtained from $\mathrm{Im}(-1/\varepsilon)$ using the KK analysis (Eq. 6) the energy-loss function has to be scaled with the help of the index of refraction (Eq. 7) which is $n = 2{\cdot}1$ in the case of AlN. To avoid extensive integrations an FFT-based KK analysis is used (Johnson, 1975). Knowledge of all frequencies is required for KK analysis but only a finite energy interval is measured (0–80 eV). Therefore the experimental data were extended up to 1000 eV using a power law of the form AE^{-r}. r was set to 3 because the fall-off of intensity should vary roughly as E^{-3} for large E (see Table 1), ignoring the logarithmic term in Eq. (1). The spectrum was truncated at 70 eV to exclude the Al L-edge where $S(E)$ does not obey the power law. The result of the KK analysis is shown in Fig. 3. The dielectric function

[1] EL/P is a software package for acquiring and processing EELS-spectra from the PEELS. It is available from Gatan Incorporated, 6678 Owens Drive, Pleasanton, CA 94566, U.S.A.

[2] GRAMS/386 is a 32-bit PC-based spectroscopy environment which supplies a vectorized programming language. Veels.ab and KKeels.ab are tools for the analysis of VEEL spectra which are developed in the GRAMS environment. GRAMS/386 is available from Galactic Industries, 325 Main Street, Salem, NH 03079, U.S.A. Veels.ab and KKeels.ab are available from Spectrum Squared Associates, 755 Snyder Hill Road, Ithaca, NY 14850, U.S.A.

[3] The mathematician K. Pearson organized (in the years 1890–1900) a system for describing 'families' of distributions. The system describes probability density functions p as solutions of the equation $(1/p)(\mathrm{d}p/\mathrm{d}x) = -(a+x)/(c_0 + c_1x + c_2x^2)$. A family (Pearson I, II, etc.) is characterized by the values of a, c_0, c_1, c_2. The Pearson VII family has $a = c_1 = 0$, $c_0 > 0$, $c_2 > 0$.

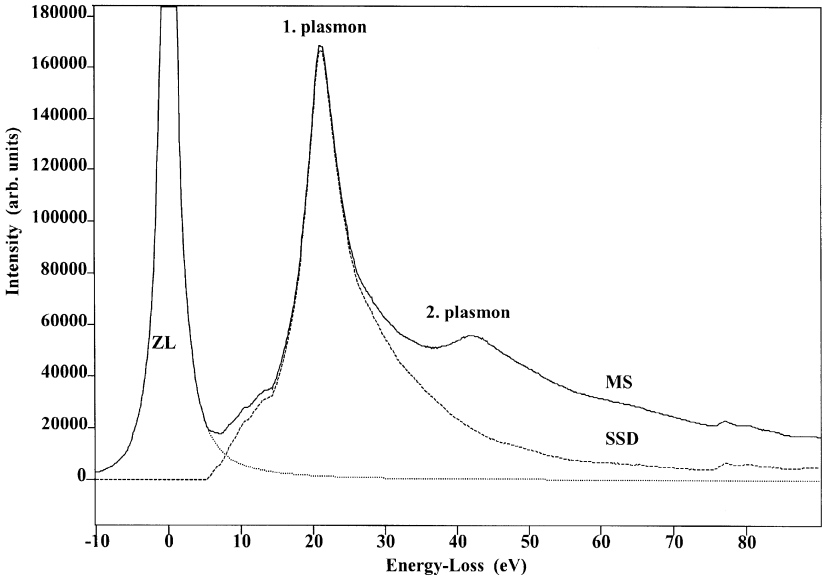

Fig. 2. Single scattering energy-loss spectrum (SSD) for single-crystal AlN determined by single scattering deconvolution of the multiple scattering energy-loss spectrum (MS). Also shown is the zero-loss peak (ZL) with the fitted zero-loss peak wing extension. Note the second plasmon peak evident at 40 eV, which is not evident in the single scattering distribution.

$\varepsilon = \varepsilon_1 + i\varepsilon_2$ was calculated from $\mathrm{Re}(1/\varepsilon)$ and $\mathrm{Im}(-1/\varepsilon)$ by simple algebra.

4.4. J_{CV} and sum rules

The determination of $J_{CV}(E)$ and $n_{eff}(E)$ is straightforward using Eqs (11) and (13). The effective number of electrons provides a check on the data. This number should never exceed the number of valence electrons for an energy that is below the first inner-shell ionization energy. The interband transition strength of single crystal AlN is shown in Figs. 4 and 5. J_{CV} is plotted against the transition energy E which corresponds to the energy loss of the experimental spectra. The optical sum rule is plotted in Fig. 6.

The interband transition strength of polycrystalline AlN is not shown here but these results agree with those from the single crystal AlN within the accuracy of the method. The spectra were obtained from a single grain of the polycrystalline specimen because the grain size is much bigger than the volume which was irradiated with the electron beam.

5. Discussion

5.1. Influence of experimental parameters

In this section the influence of the experimental parameters on the results, and the difficulties are discussed. Several series of EEL-spectra have been acquired where the

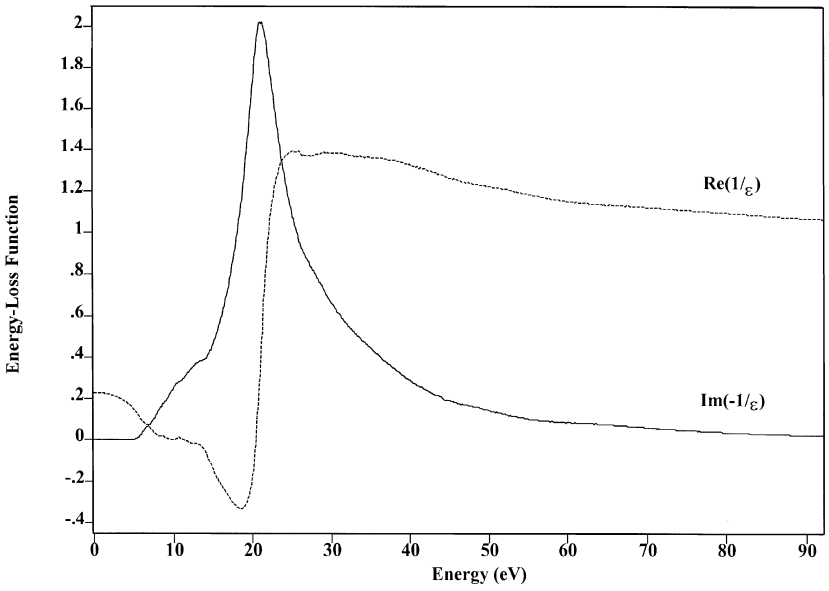

Fig. 3. Energy-loss function $\mathrm{Im}(-1/\varepsilon)$ of single-crystal AlN, on an absolute scale determined using the index sum rule, and $\mathrm{Re}(1/\varepsilon)$ determined by Kramers–Kronig dispersion analysis.

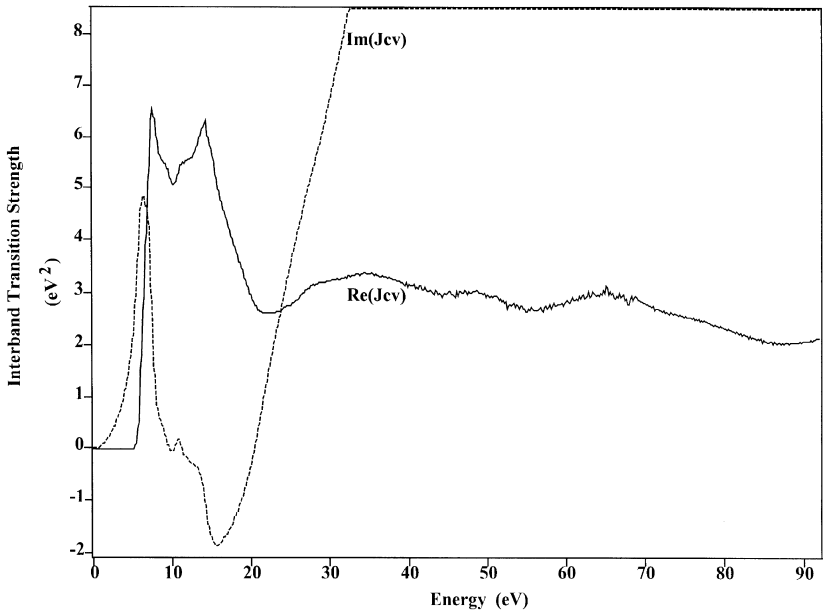

Fig. 4. Interband transition strength of single-crystal AlN, where the absorptive component is given by Re(J_{CV}) and the dispersive component is given by Im(J_{CV}).

convergence and collection semi-angles have been varied from 6·5 to 25 mrad and from 3·3 to 13 mrad, respectively, by the choice of the objective and collector aperture (Pfleiderer, 1996). It appeared that these parameters did not affect the lineshape of $J_{CV}(E)$ significantly and the peak positions were found to be shifted by less than 0·2 eV. A second result was that no influence of the orientation of the crystal with respect to the incident electron beam on $J_{CV}(E)$ was evident. This can be interpreted as a result of the low anisotropy of the dielectric function of AlN as deduced from the indices of refraction (3% difference for the direction parallel and orthogonal to the *c*-axis of the crystal). Because the TEM-specimen is wedge-shaped it is possible to choose areas of different thicknesses from where the EEL-spectra were taken from. The value of $J_{CV}(E)$ at the first peak at 7·5 eV increased systematically with decreasing thickness up to 12·2 eV^2 for $t = 25{\cdot}4$ nm. We believe that this is an effect of an oxygen-rich surface layer of the order of 2 nm on the both sides of the specimen. (The thickness of the oxygen layer was determined from the intensity of the O K-edge and assuming the oxide to be alumina.) This layer has a negligible contribution to the spectrum if the sample has

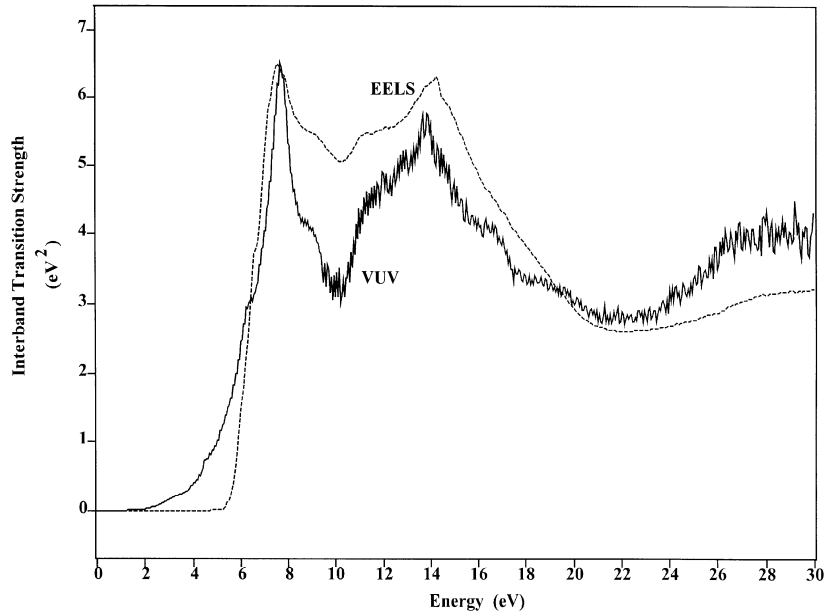

Fig. 5. Comparison of the real part of the interband transition strength Re(J_{CV}) of AlN determined by VEELS and VUV-spectroscopy.

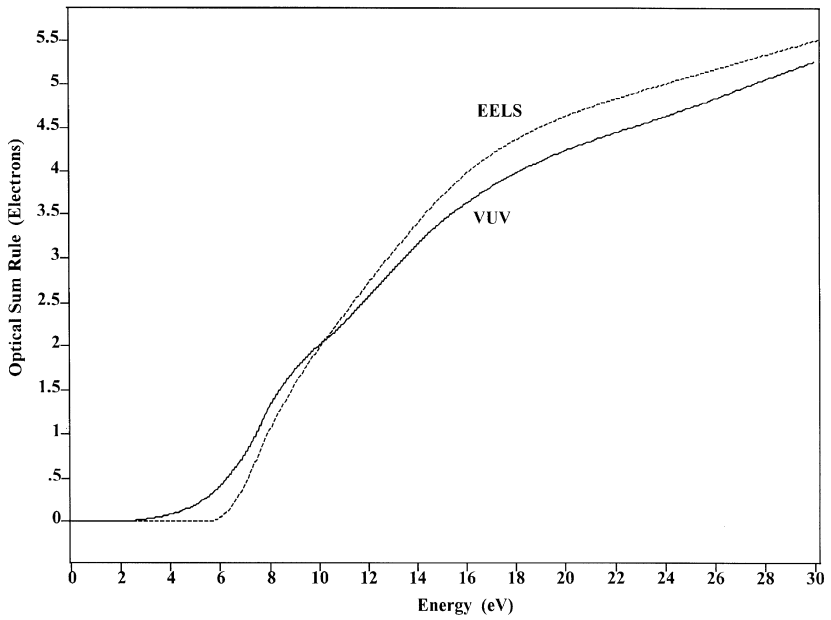

Fig. 6. Comparison of the oscillator strength sum rule (Eq. 13) of AlN from the experimental VEELS and VUV-spectroscopy.

a thickness of about one mean free path as was used here.

5.2. Comparison with VUV results

The comparison of the interband transition strength $J_{CV}(E)$ and the effective number of electrons determined from VEELS and from VUV-spectroscopy is shown in Figs 5 and 6. The VUV-measurements and the analysis of the reflectivity were performed by Loughin (1992). The polycrystalline AlN which is identified as sample no. 300 in that work had been exposed to moisture during surface preparation (aqueous polish). They show a good agreement in the interband transition strength considering the positions of the maxima at 7·5 and 14·2 eV and the minimum at 10·2 eV. Both results agree on an absolute scale, except that the minimum at 10·2 eV is lower for the VUV-results. Note that these results are obtained from two experiments based on two different physical principles. In EELS, electrons serve as a probe of the interband transitions and the valence electronic structure, whereas VUV-spectroscopy measures the reflectivity for light. Because the energy resolution of VUV-spectroscopy is better (3–100 meV at energies of 3·5–35 eV) the features in J_{CV} determined by VEELS are less sharp and appear broadened.

The agreement between the VEELS and VUV results can be demonstrated quantitatively by considering the critical point model parameters shown in Table 2. Both VEELS and VUV interband transition strengths can be described by the same number and types of critical points: one 2D set, one

Table 2. Critical point model parameters and sum rule for the different sets of transitions in AlN from VEELS and VUV results.

Critical point set	Critical point type	VEELS energy (eV)	VUV energy (eV)	VEELS n_{eff}	VUV n_{eff}
1	D_0	6·0	5·8	1·4	1·5
1	D_1	7·5	7·7		
1	D_2	9·7	9·4		
2	M_0	8·9	8·9	3·1	2·8
2	M_1	11·0	11·2		
2	M_2	14·4	14·1		
2	M_3	21·3	21·3		
3	S_0	29·6	29·5	0·9	1·0
			Total	5·4	5·3

3D set and one 0D set The energies of the critical points corresponding to the first set differ typically by 0·2 eV and only for one critical point by 0·3 eV. The partial sum rules of the three sets of critical points agree as well. The contribution of the second set of critical points to the total number of electrons undergoing a transition is about double that of the first, and three times that of the third set in both cases.

The critical point model embodies the topology of the material's band structure as opposed to being just a parametric fitting procedure. The critical point model parameters do not correspond only to the energy of the peaks but to the complete shape of the J_{CV}. Therefore the close agreement between the two critical point models, for VEELS and VUV data, indicates that, instrumental contributions aside, the two techniques reveal comparable information about the electronic structure of AlN.

The sum rule does not reach the value of 8, corresponding to the total number of valence electrons per unit formula in AlN, because the integral is extended only to 30 eV. This indicates that there are transitions at higher energies involving the valence electrons. This is a well-known phenomenon in EEL-spectroscopy since the background in front of and underlying the core absorption edges arises from inelastic scattering of the fast electrons with the valence electrons of the material. The differences in the total number of electrons between the sum of the three balanced sets (Table 2) and the integral over the experimental data (Fig. 6) arises from the details of the fit of the critical point model to the experimental data.

A comparison to VUV-data of non-aqueous polished AlN where moisture was strictly avoided shows some differences from the aqueous polished VUV- and the VEELS-results. The critical point model of this sample consists of three sets of balanced critical points which differ in number, type and energy from the model shown in Table 2 (Loughin *et al.*, 1996). The reason for this is not yet fully understood. One possible explanation is that the electronic structure of AlN is changed by the contact with water during sample preparation in the case of VUV (aqueous polish) and EELS.

The agreement of the results after aqueous preparation leads to a number of conclusions: the dipole approximation is valid up to several mrad for VEELS of AlN. The collection semi-angle of 13 mrad corresponds to a momentum transfer of $22{\cdot}1\ \mathrm{nm}^{-1}$ (Eq. 2) for an energy loss of $E = 20$ eV which is in the order of the first Brillouin zone. A possible explanation for this is that the electrons which are scattered into small angles have the biggest contribution to the spectrum because the differential cross-section declines as θ^{-2} for high scattering angles. Another fact which can be derived from the agreement is that the Cerenkov radiation can be neglected in the case of AlN. Radiation losses have been studied under different conditions for III–V compounds such as AlN (Daniels *et al.*, 1970).

6. Conclusions

The quantitative analysis of VEELS of AlN has been performed to determine the interband transition strength J_{CV}. A critical point model of J_{CV} was constructed and compared with the results of more established VUV-spectroscopy. The good agreement of the results obtained by both techniques leads to the conclusion that VEELS is a reliable method for the determination of the electronic structure of materials. We believe that the knowledge of both the experimental technique and the analysis is developed in a way that makes VEELS a tool which can be used independently of other methods. Therefore, VEELS analysis provides a new method to study dielectric properties, electronic structure and bonding of bulk material. One advantage is the possibility to investigate internal interfaces (and other crystal defects) directly because of the high spatial resolution available in a dedicated STEM.

Acknowledgments

We thank M. Sycha for preparing the TEM specimen, J. Thomas for assistance with the electron microscope and the spectrometer and Professor G. A. Slack for providing the single crystal sample. We are grateful to Dr L. K. DeNoyer and Dr G. Duscher for software development and to R. Youngman and P. Redlich for discussion. Harald Müllejans acknowledges the financial support of the Volkswagen-Stiftung (contract I/70082).

References

Ching, W.Y. (1990) Theoretical studies of the electronic properties of ceramic materials. *J. Am. Ceram. Soc.* **73,** 3135–3160.

Ching, W.Y. & Harmon, B.N. (1986) Electronic structure of AlN. *Phys Rev. B*, **34**, 5305–5308.

Daniels, J., Festenberg, C., Raether, H. & Zeppenfeld, K. (1970) Optical constants of solids by electron spectroscopy. *Springer Tracts Mod. Phys.* **54,** 77–135.

Egerton, R.F. (1996) *Electron Energy-loss Spectroscopy in the Electron Microscope*, 2nd edn. Plenum, New York.

Egerton, R.F., Yang, Y.Y. & Cheng, S.C. (1993) Characterization and use of the Gatan 666 parallel-recording electron energy-loss spectrometer. *Ultramicroscopy,* **48,** 239–250.

Festenberg, C. (1969) Energieverlustmessungen an III–V-Verbindungen. *Z. Physik*, **227**, 453–481.

Fink, J. (1989) Recent developments in energy-loss spectroscopy. *Adv. Electron. Electron Phys.* **75,** 121–232.

French, R.H. (1990) Electronic band structure of Al_2O_3, with comparison to AlON and AlN. *J. Am. Ceram. Soc.* **73,** 477–489.

French, R.H., Cannon, R.M., DeNoyer, L.K. & Chiang, Y.-M. (1995) Full spectral calculation of non-retarded Hamaker constants for ceramic systems from interband transition strengths. *Solid State Ionics*, **75,** 13–33.

French, R.H., Jones, D.J. & Loughin, S. (1994) Interband electronic structure of α-alumina up to 2167 K. *J. Am. Ceram. Soc.* **77,** 412–422.

French, R.H., Müllejans, H., Jones, D.J., Duscher, G., Cannon, R.M. & Rühle, M. (1998) Dispersion forces and Hamaker constants for intergranular films in silicon nitride from spatially resolved-valence energy loss spectrum imaging. *Acta Mater.* **46**, 2271–2287.

Gautier, M., Duraud, J.P. & Le Gressus, C. (1987) Electronic structure of an AlN film produced by ion implantation, studied by electron spectroscopy. *J. Appl. Phys.* **61,** 574–580.

Johnson, D.W. (1975) A Fourier series method for numerical Kramers-Kronig analysis. *J. Phys. A: Math. Gen.* **8,** 490–495.

Johnson, N.L. & Kotz, S. (1970) *Distributions in Statistics: Continuous Univariate Distributions*, Vol. 1, p. 13. Houghton Mifflin Company, Boston.

Kramers, H.A. (1927) La diffusion de la lumière par les atomes. *Atti. Congr. Int. Fis. Como.* **2,** 545–557.

de Kronig, R.L. (1926) On the theory of dispersion of X-rays. *J. Opt. Soc. Am.* **12,** 547–557.

Lieske, N. & Hezel, R. (1981) Formation of Al-nitride films at room temperature by nitrogen ion implantation into aluminum. *J. Appl. Phys.* **52,** 5806–5810.

Loughin, S. (1992) *Vacuum ultraviolet spectroscopy and analytical critical point modeling of the electronic structure of aluminum nitride.* Dissertation, University of Pennsylvania.

Loughin, S., French, R.H., Ching, W.Y., Xu, Y.N. & Slack, G.A. (1993) Electronic structure of aluminum nitride: theory and experiment. *Appl. Phys. Lett.* **63,** 1182–1184.

Loughin, S., French, R.H., DeNoyer, L.K., Ching, W.Y. & Xu, Y.N. (1996) Critical point analysis of the interband transition strength of electrons. *J. Phys. D: Appl. Phys.* **29,** 1740–1750.

Müllejans, H., Bruley, J., French, R.H. & Morris, P.A. (1993) Quantitative electronic structure analysis of α-Al_2O_3 using spatially resolved valence electron energy-loss spectra. *IOP Conf. Ser.* **138,** 59–62.

Müllejans, H., Bruley, J., French, R.H. & Morris, P.A. (1994) Quantitative electronic structure analysis of α-Al_2O_3 using spatially resolved valence electron energy-loss spectra. *Mater. Res. Soc. Proc. Symp.* **332,** 169–176.

Müllejans, H. & French, R.H. (1996) Interband electronic structure of a near Σ11 grain boundary in α-alumina determined by spatially resolved valence electron energy-loss spectroscopy. *J. Phys D: Appl. Phys.* **29,** 1751–1760.

Olson, C.G., Sexton, J.H., Lynch, D.W., Bevolo, A.J., Shanks, H.R., Harmon, B.N., Ching, W.Y. & Wieliczka, D.M. (1985) Photoelectron and electron energy-loss spectra of epitaxial aluminum nitride. *Solid State Commun.* **56,** 35–37.

Pfleiderer, A. (1996) *Ortsaufgelöste Elektronenenergieverlustspektroskopie von inneren Grenzflächen in Keramiken.* Diplomarbeit, Universität Stuttgart.

Raether, H. (1965) Solid state excitations by electrons. *Springer Tracts Mod. Phys.* **38,** 84–157.

Schattschneider, P. (1986) *Fundamentals of Inelastic Electron Scattering.* Springer, Wien.

Slack, G.A. (1973) Nonmetallic crystals with high thermal conductivity. *J. Phys. Chem. Solids*, **34,** 321–335.

Smith, D.Y. (1985) Dispersion theory, sum rules, and their application to the analysis of optical data. *Handbook of Optical Constants of Solids* (ed. by E. D. Palik), pp. 35–68. Academic Press, New York.

Sutton, A.P. (1993) *Electronic Structure of Materials.* Clarendon Press, Oxford.

Walsh, C.A. (1989) *Modelling and interpretation of electron energy-loss spectra from interfaces*. Dissertation, University of Cambridge.

Werdecker, W. & Aldinger, F. (1984) Aluminum nitride – an alternative ceramic substrate for high power applications in microcircuits. *IEEE Trans. Components, Hybrids, Manuf. Technol.* **7,** 399–404.

Wooten, F. (1972) *Optical Properties of Solids.* Academic Press, New York.